CONSTRAINED HYDRAULIC FRACTURE OPTIMIZATION FRAMEWORK

Mei Yang[1], Aura Araque-Martinez[1], Nnamdi Abolo[1]

1: Weatherford International. mei.yang@weatherford.com, aura.araque@weatherford.com, namdiabolo@gmail.com

Keywords: **Hydraulic Fracture, Fracture Geometry, Unconventional Play, Completion, Optimization**

RESUMEN

Metodología de trabajo integrada para la optimización de fracturas hidráulicas
Pozos horizontales con múltiples fracturas, se han convertido en el método de estimulación más usado para producir yacimientos no convencionales que están caracterizados por bajas y extremadamente bajas permeabilidades. El comportamiento de pozos en este tipo de yacimientos está definido por un largo periodo de flujo lineal transitorio, el cual depende de la ya conocida relación entre el área de fractura y la permeabilidad: $A_f\sqrt{k}$, por lo tanto; una sobre estimación del área de fractura trae como consecuencia una subestimación de la permeabilidad y viceversa. En base a esto, existe la necesidad de una estimación del área de fractura lo más preciso posible, a fin de reducir la incertidumbre en la permeabilidad del yacimiento.
Este artículo presenta un flujograma sistemático de trabajo que integra la data dinámica y estática a fin de optimizar la completación del pozo y determinar el área efectiva de fractura. El flujo de trabajo incluye cuatro (4) niveles diferentes de integración, los cuales se discuten en este trabajo.
La aplicación del flujograma propuesto también es presentada en este trabajo, utilizando los datos de un pozo completado en la formación Marcellus. Los resultados, validan la importancia de la integración de la data pertinente en este tipo de yacimientos a fin de optimizar las completaciones y determinar el área efectiva de fractura.

INTRODUCTION

The unconventional reservoirs development depends greatly on economics; and that is the main reason for the industry focus on completion optimization processes. For years numerous people have researched on this topic. Roberts (1981) and Ventura (1985) worked on evaluating past fracture data to develop an optimization program for specific plays. Richardson (2000) presented his method to predict fracture half-length based on a good estimate of fracture conductivity. Soliman *et al.* (2004), Agiddi *et al.* (2005), Rahman *et al.* (2006), Jamiolahmady *et al.* (2009), Cipolla *et al.* (2011), Pitakbunkate *et al.* (2011), Rahman *et al.* (2011), Shebl *et al.* (2012), Yang *et al.* (2012), Jin *et al.* (2013), Brake *et al.* (2013), Taylor *et al.* (2013), Saldundaray *et al.* (2013), and Ugueto *et al.* (2014), have focused on more rigorous workflows to optimize fracture designs based on reservoir conditions and economics. Brake *et al.* (2013) showed the importance of integrating field results and surveillance data to optimize fracture stimulation treatments in Wamsutter field. Ugueto *et al.* (2014) showed how complementary diagnostics from different data sources help to reduce uncertainty to optimize completion designs. The majority of these works are based on large data sets from past fracture treatments and there is still a need for developing a comprehensive workflow for fracture optimization integrating static and dynamic data.

This work presents an integrated approach that spans from the formation evaluation to the post frac evaluation to optimize fracture designs. This framework begins with the reservoir characterization step based on logs and core/cuttings analysis and interpretation. This is followed by building the preliminary geomechanical model as the second step. Next, the fracture model is compared to Microseismic data if available. Finally, the constrained fracture model is calibrated against performance data to actually determine the effective fracture area.

The integrated hydraulic fracture calibration framework discussed in this paper is a robust method to systematically design hydraulic fracture, by determining the effective fracture area. This is valuable information to reduce uncertainty in the estimation of the reservoir permeability, EUR, the estimated stimulated reservoir volume (SRV), the well spacing and fracture spacing.

COMPLETION OPTIMIZATION FRAMEWORK

The proposed framework comprises four (4) different levels of integration as presented in Figure 1 and follows the four-step approach. Details of each step are discussed in the following paragraphs:

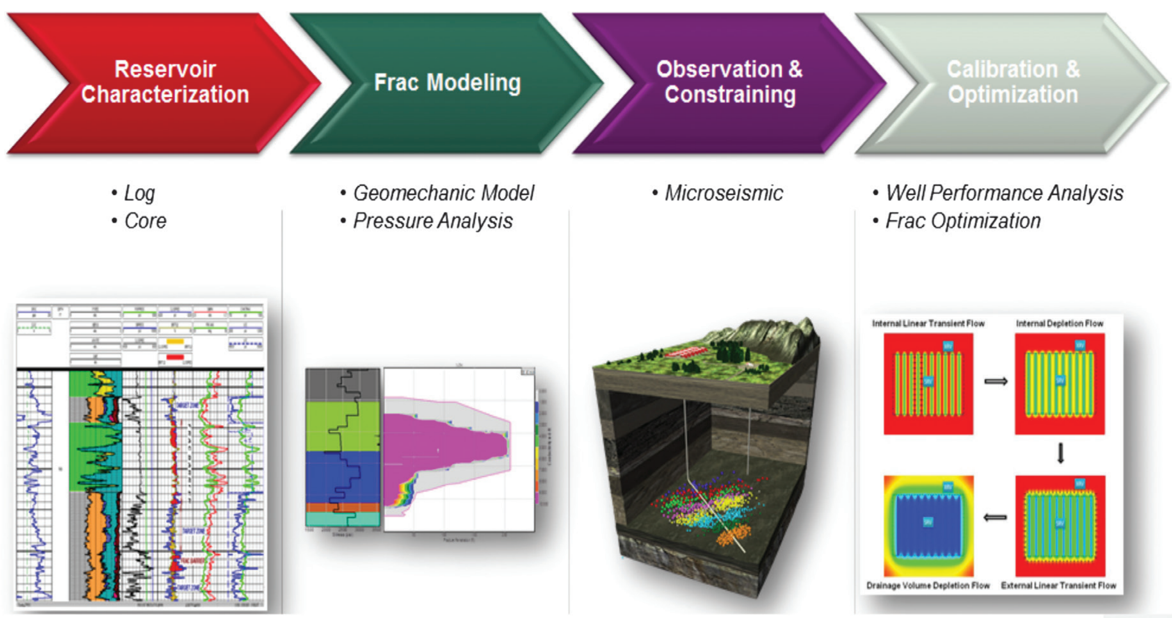

Figure 1. Completion optimization framework.

- **Step 1: Reservoir Characterization**. This step integrates log and core data to better understand the reservoir. In this unconventional plays productivity is not only a function of geology but also completion. Therefore; rock and reservoir quality evaluation is key to optimize well's completion. In this case, rock quality refers to how brittle or ductile the specific interval is. A relative brittle zone is easier to be hydraulic fractured comparing to a ductile zone. A comparison of Young's modulus and Poisson's ratio is used to evaluate the rock quality as shown in Figure 2. Reservoir quality refers to the hydrocarbon content along the target zone. The reservoir's potential and lithology is evaluated by using core and log data.

A well in these unconventional plays should be placed in the zone where the high production potential zones, i.e, good reservoir quality or pay zones, are accessible through hydraulic fracture. Figure 3 shows the reservoir quality evaluation results for a sample well in the Marcellus shale identifying the zones with best reservoir quality, *i.e.*, high hydrocarbon content zone (track 6 & track 7), where the blue marker is upper vs. lower Marcellus zonal division.

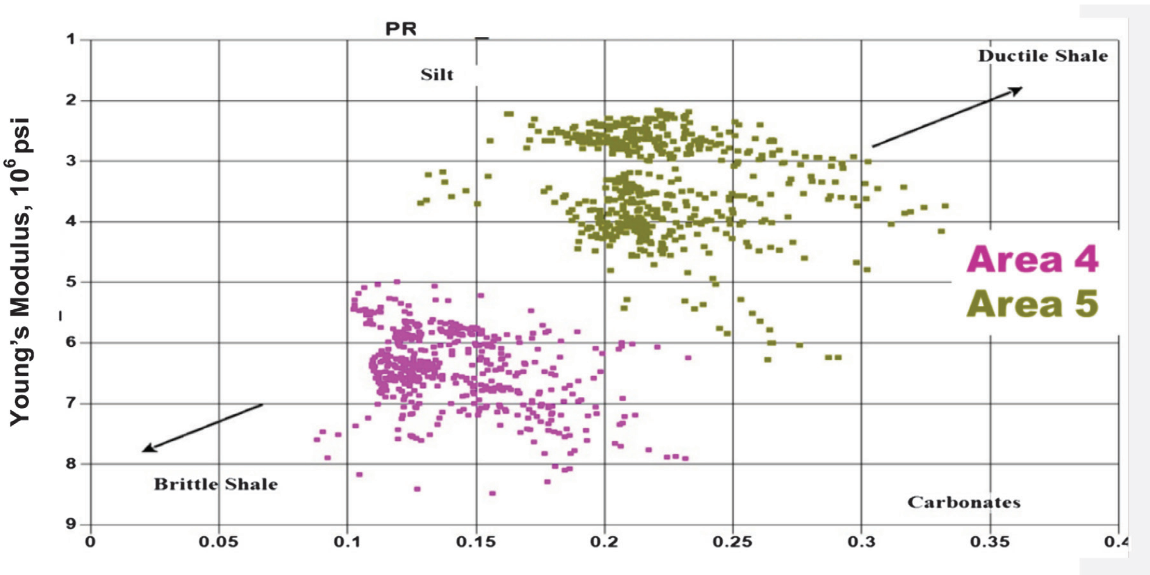

Figure 2. Young's modulus vs. Poisson's ratio for specific areas in Marcellus Shale.

- **Step 2: Hydraulic Fracture Modeling**. In this second step, we use geomechanical rock properties from reservoir characterization to model the initial fracture geometry. Specific well properties such as the number of clusters, the perforated lateral length, fluid volume, and proppant mass pumped during fracture treatment, and formation layering tops were also input in the geomechanical model. This stimulation model is such that vertical stress contrast is captured so as to accurately model the vertical growth in each fracture.

Fracture geometry, proppant placement, conductivity and width profile along the fracture is generated in this step of the proposed framework. Fractures are assumed effective only if they had

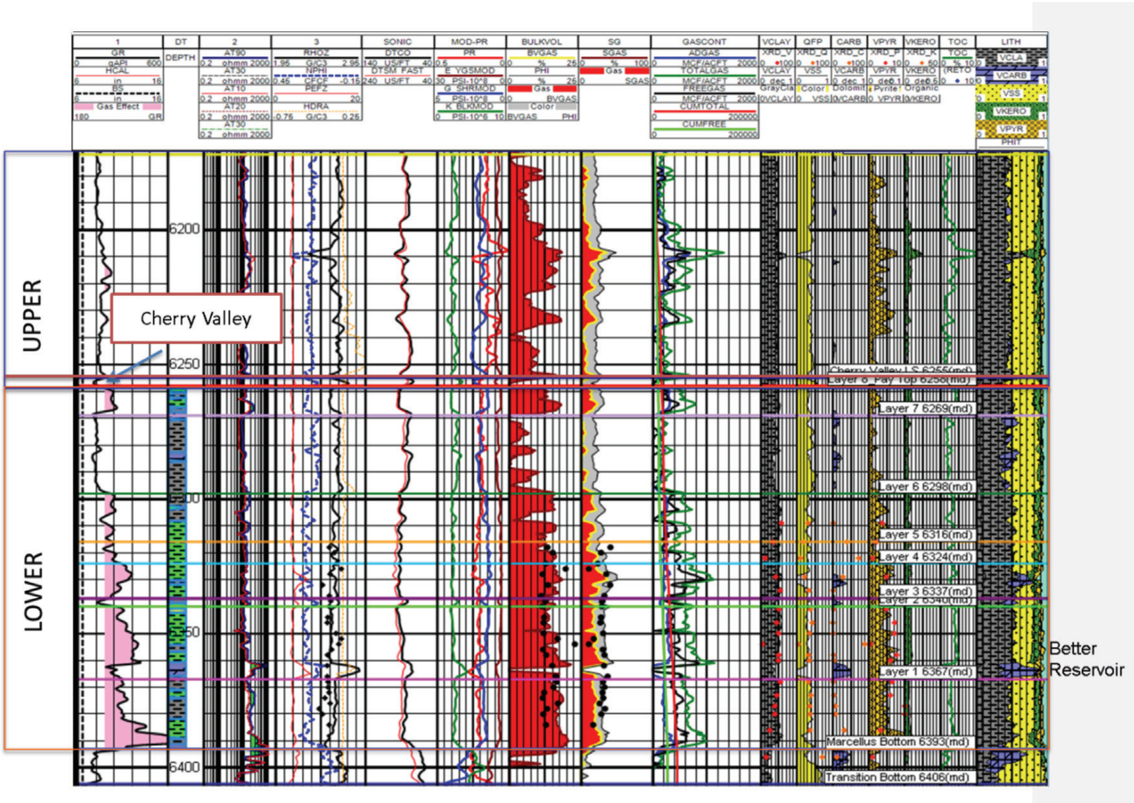

Figure 3. Log plot showing the results of a detailed petrophysical analysis.

a conductive path from the wellbore out into the reservoir greater than 1 mD-ft (Fcd = 30). The effective fracture is defined as pay which is propped and connected to the wellbore. The main fracture job pressure and rate data, Injection test, Fall off test and Step rate test if available will be used to understand closure pressure, formation leakoff, and fracture extension pressure.

- **Step 3: Observation & Constraining**. This third step integrates the initial fracture model with Microseismic information, if available. In this case, Microseismic is used to understand fracture propagation and is a good indicator of the hydraulic fracture geometry, while fracture modeling provides propped fracture geometry. Therefore; fracture dimensions generated from fracture modeling should be within the range of Microseismic results.

Realtime Microseismic monitoring can be employed for fracture job adjustment at fracture job site, along with bottomhole pressure (BHP) and injection rate to improve the completion job success rate.

- **Step 4: Calibration & Optimization.** This last step includes the post-frac evaluation to determine effective fracture area and optimize future fracture designs as shown in Figure 4. The constrained fracture geometry from previous step, is then calibrated with the performance data (rates and pressures) using a reservoir flow simulator. This will give the effective fracture geometry, which will be used to estimate the effective stimulated reservoir volume (SRV). These results will determine the fracture job effectiveness. Sensitivity studies of the following parameters, but not limited to, are performed to determine the optimum fracture design based on net-present-value (NPV) evaluation:

- Slurry
- Proppant Concentration
- Pump Rate
- Initiation Point

Each of the frac geometry from the sensitivity cases are evaluated in the flow model. NPV calculations from these forecasted cases are performed to select the optimum case. This will interpret reservoir data to inform decisions and maximize rate of investment (ROI).

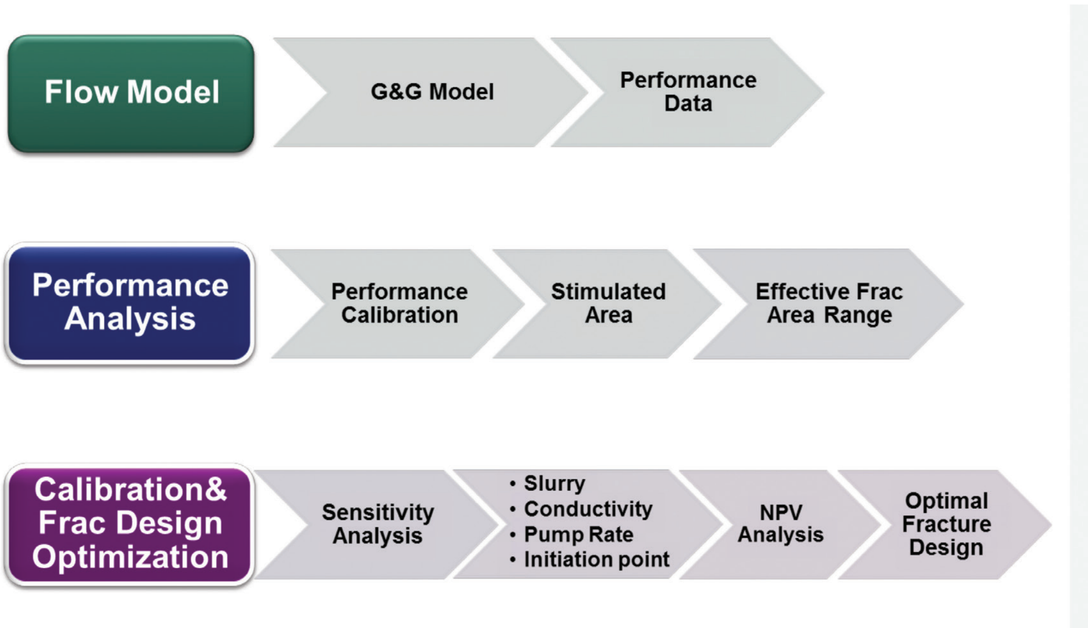

Figure 4. Model calibration and optimization.

FIELD APPLICATION

Marcellus shale was deposited in the Middle Devonian period. The excellent rock properties of high Total Organic Carbon (TOC), porosity, and permeability found in the Marcellus Shale are due to the paleogeography, and preservation of the organics by basin-wide, bloom-related anoxic events. The organic rock quality varies across relatively small areas of the basin because of the localized algal blooms. This is the reason why some regions have superior productivity.

The Marcellus is bounded on the bottom by Onondaga Limestone; there is a thin streak of Purcell/Cherry Valley limestone in the middle of the Marcellus formation. The well has been drilled between these two limestones but closer to the Onondaga Limestone.

Here we discuss a field application of the proposed framework in one well in Marcellus field. Details are as follows:

- **Step 1: Reservoir characterization**

In this case, no logs were available for the study well, therefore; the petrophysical analysis was based on the logs from the closest offset wells, within 5 miles away from the treatment well. These well logs provided by the client were corrected for environmental effects on logging tools and then used in association with information gathered from core analyses to conduct petrophysical formation evaluation. The core data provided included core desorption and methane gas isotherms, gas analyses, XRD, core geochemistry, and rock mechanics measurements (Young's Modulus and Poisson's ratio) on core samples. The reservoir porosity and Sw in the Marcellus wells were obtained from transforms of bulk density based on core analysis. The objective of the petrophysical analysis was to evaluate the Marcellus formation for porosity, lithology, gas-filled porosity, gas saturation, total organic carbon, and gas in-place.

Specialized logs such as sonic shear and compressional were correlated based on the available information from surrounded wells. The mud systems in the vertical section are mostly water-based mud with a reported mud density of 9.7 lbs/gal. Well logs maximum recorded bottomhole temperature was approximately 125-130°F (52-54oC). Main petrophysical parameters are shown in Table 1.

Petrophysical Units	Value
Porosity (%)	4.8
Net to Gross ratio (%)	63
Water Saturation (%)	42
Gross Thickness (ft)	336
Langmuir Volume (scf/ton)	55
Langmuir Pressure (psia)	523
Total Original Gas In Place(Bscf/section)	53
Free Original Gas In Place(Bscf/section)	31
Adsorbed Original Gas In Place(Bscf/section)	22

Table 1. Petrophysical Properties.

In general, the Marcellus formation is divided into 2 main units: Upper Marcellus and Lower Marcellus. We further divided the Lower Marcellus into 8 different units based on change of facies. Unit 1 is the bottom layer and Unit 8 is the Lower Marcellus top or pay top. Lower portion of lower Marcellus was identified as the best reservoir quality because of the high gas content.

- **Step 2: Hydraulic fracture modeling**

The study well 1 has a 3,495-ft lateral with 12 fracture stages, with 3 perforation clusters each spaced approximately 65 - 70 ft while the fracture stages are 170-200 ft apart. Each treatment stage consisted of approximately 5,000 bbls of clean fluid. The proppants used were 100 mesh sand and 40/70 mesh sand totaling 5.0 MM-lb. Proppants was not pumped in Stage1, therefore; hydraulic width disappears after fracture closure.

Fracture modeling was carried out with available post-fracture data for each stage with the following assumptions made in fracture modeling:

- Microseismic evaluations completed on this well were used to Quality Check (QC) the fluid leak-off coefficient (0.0007 ft/min1/2).
- A fracture conductivity value of 1 mD-ft has been used as a criterion to evaluate whether the fracture is connected to the wellbore or not. This is based on embedment near wellbore (cell midpoint is 15 ft, permeability is less than 100 nD in most cases, and damage due to embedment is 95%) or no damage and a dimensionless conductivity (Fcd) of 30 at 600 ft and like permeability.
- The post-closure conductivity will be used to replicate conditions during production. No damage has been applied to the proppant pack, such as embedment.

The static Young's modulus and the stress profile were calculated as shown in Table 2. The geomechanical model was built with a dipole sonic and bulk density log constrained by core geomechanical lab results in the same wellbore. Vertically, there are layers of higher closure stress and modulus contrast: Onondaga and Cherry Valley limestone both are relatively ductile to Marcellus shale, with high closure stresses, which lessen vertical growth; there are thick layers with contrasts greater than 100 psi.

Property	Hamilton	Marcellus	Onondaga
Young's modulus (10^6 psi)	3.3	2.85	3.61
Closure pressure gradient (psi/ft)	0.75	0.73	0.75
Leak-off coefficient (ft/min$^{1/2}$)	0.0007	0.0007	0.0007

Table 2. Geomechanical model.

Results from fracture modeling are presented in Table 3 as the weighted average fracture geometry by stage. Initial fracture modeling results showed that:

- Upon applying the conductivity cut-off, the fracture modeling indicates most of the clusters appear to be contributing to the performance.
- Most fractures grow from the transition between Marcellus and Onondaga limestone to Hamilton.
- Figure 5 shows the fracture geometry of the hydraulic fractures created for a typical stage, Stage 3 in this case. It shows the variation of fracture half length, height and width in that particular stage from 3 clusters, including the conductivity profile.
- The inner fractures grow lower due to the stress shadows overcoming the local stress

barriers. The frac width is narrower in the inner fracs while it is wider in the outer fracs with low closure stress.

- The hydraulic fracs grow upward a few hundred feet into the Hamilton since there is little vertical stress contrast.

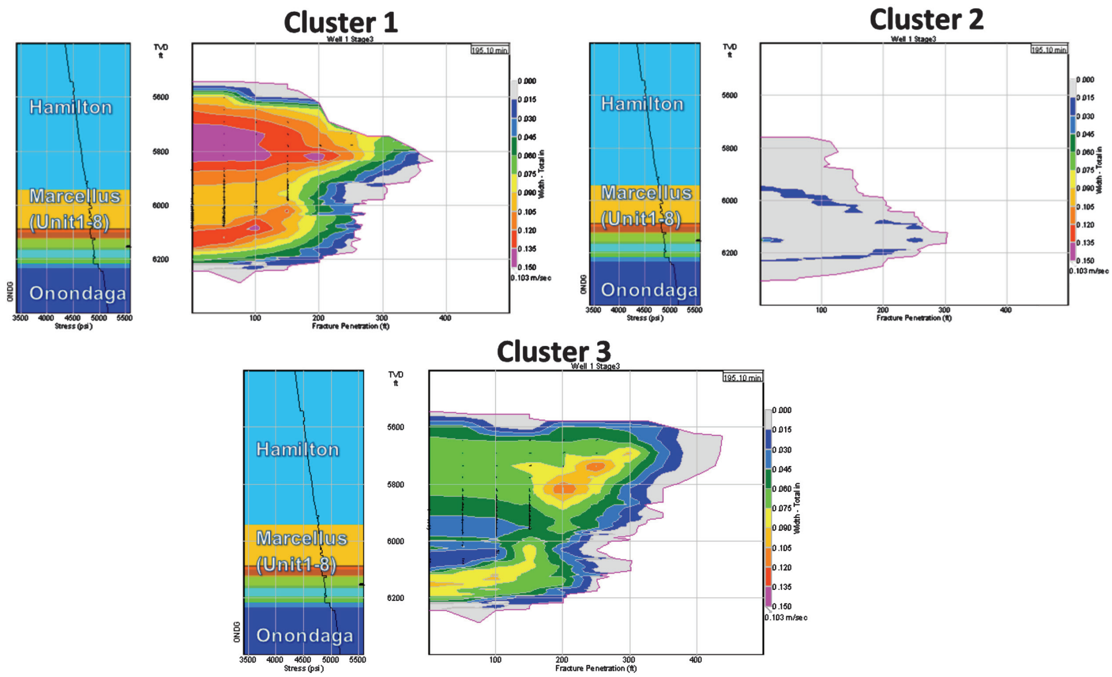

Figure 5. Well1 Stage fracture geometry and conductivity profile.

Stg	# of clusters	Fracture Height(ft)			Fracture Half-Length (ft)			Min Frac Area (ft^2)	Max Frac Area (ft^2)
		Min	Max	Avg	Min	Max	Avg		
1	0	0	0	0	0	0	0	0	0
2	3	464	576	507	201	458	340	559,356	1,324,020
3	2	171	400	286	247	265	253	181,296	395,908
4	3	99	468	233	62	340	313	49,104	953,856
5	3	172	595	331	164	304	277	223,236	1,083,768
6	3	464	569	523	201	493	370	559,668	1,583,700
7	3	391	597	503	217	362	298	664,746	1,134,600
8	3	146	527	374	270	286	279	236,112	872,832
9	3	176	472	278	256	573	442	560,952	725,346
10	3	141	596	402	267	406	343	225,972	1,141,104
11	3	446	512	484	261	324	296	773,700	919,548
12	2	473	583	528	237	334	289	552,632	632,712
Fracture Area,ft^2		Min	4,586,774		Avg	8,035,903		Max	10,767,394

Table 3. Initial Geomechanical Model.

- **Step 3: Observation & Constraining**

Microseismic observation is integrated with the fracture modeling results at this step. Figure 6 and Figure 7 shows the Microseismic interpretation on this well. One key reason to model the well was to match the interpretations for the hydraulic fracture half-length and vertical growth. Table 4 shows the Microseismic interpretation on this well. Results show that geomechanical model is within the range of Microseismic registered events, therefore; no further constrain needs to be applied. Also, the difference columns in Table 4, especially the highlighted cells, illustrate data should be validated from multiple data resources. Microseismic shows crack events in stage 1 while in this stage, since no proppants were pumped, fractures will be closed after job.

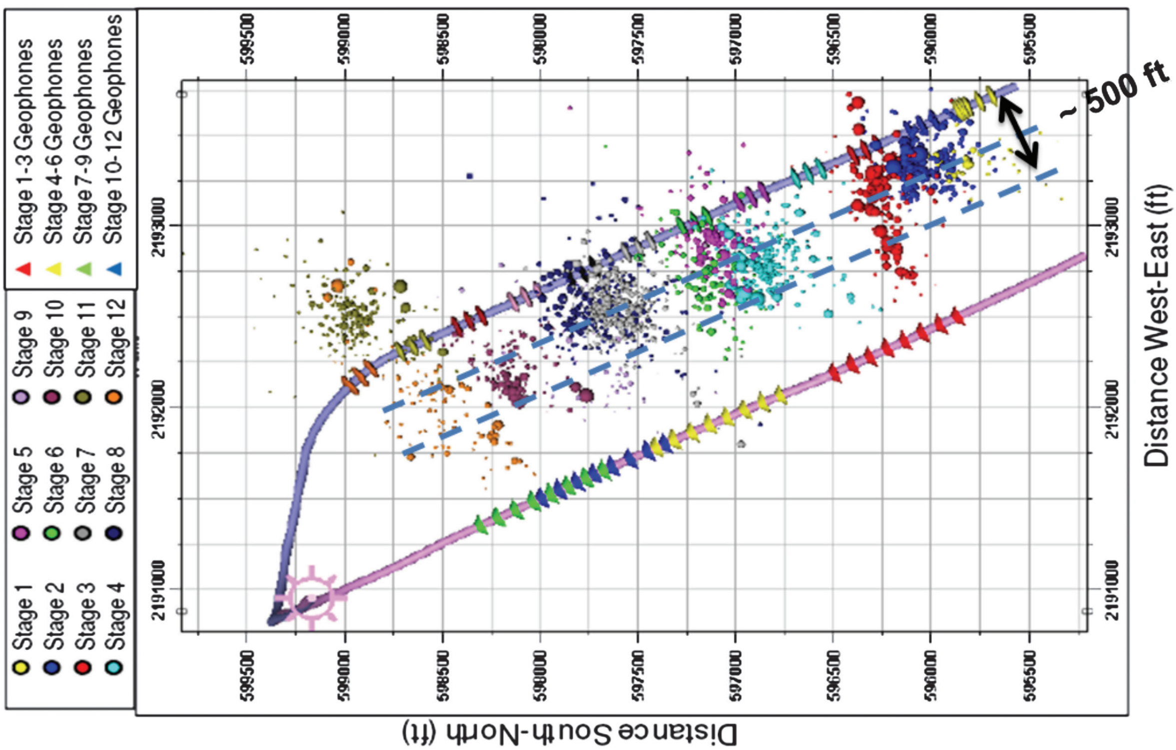

Figure 6. Microseismic interpretation – Areal View: Fracture horizontal growth.

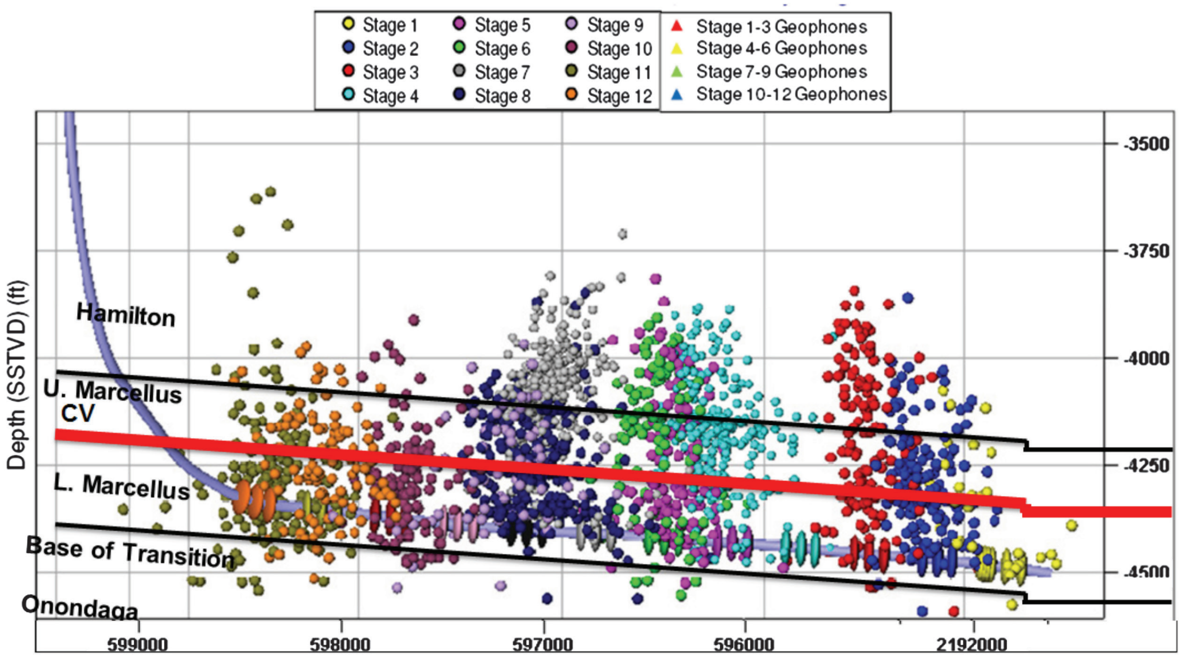

Figure 7. Microseismic interpretation – Vertical View: Fracture vertical growth.

Fracture Geometry	Estimation from Microseismic		
	Fracture Height	Half Length, ft	Area, ft2
Stage 1	350	250	525,000
Stage 2	500	250	750,000
Stage 3	625	500	1,875,000
Stage 4	625	400	1,500,000
Stage 5	625	400	1,500,000
Stage 6	625	600	2,250,000
Stage 7	625	500	1,875,000
Stage 8	625	300	1,125,000
Stage 9	500	500	1,500,000
Stage 10	350	600	1,260,000
Stage 11	500	500	1,500,000
Stage 12	625	500	1,875,000
Total			17,535,000

Table 4. Microseismic Fracture Geometry.

- **Step 4: Calibration & Optimization**

This step is essential to understand the effective fracture area and reservoir properties. Upon honoring the fracture properties for each fracture model, well performance was calibrated to the history data. The performance match for this scenario is presented in the Figure 8. Although the results look acceptable, further simulation runs were carried out to improve the match and evaluate the effect of fracture area estimation. In this case, a much better history match was obtained by substantially reducing the frac area from Table 3 and slightly increasing the frac conductivity as shown in Figure 9. This adjustment was based on the value of the $A_f \sqrt{k}$ derived from the linear transient flow evaluation. Based on this relationship there is a value of fracture area for each permeability value. These results show that the pre-constrained model could overestimate the fracture area, which may cause an underestimation in the reservoir permeability. By integrating different data sources as constrains, a more accurate model is built that provides a better relationship between effective fracture geometry and reservoir permeability for the studied field.

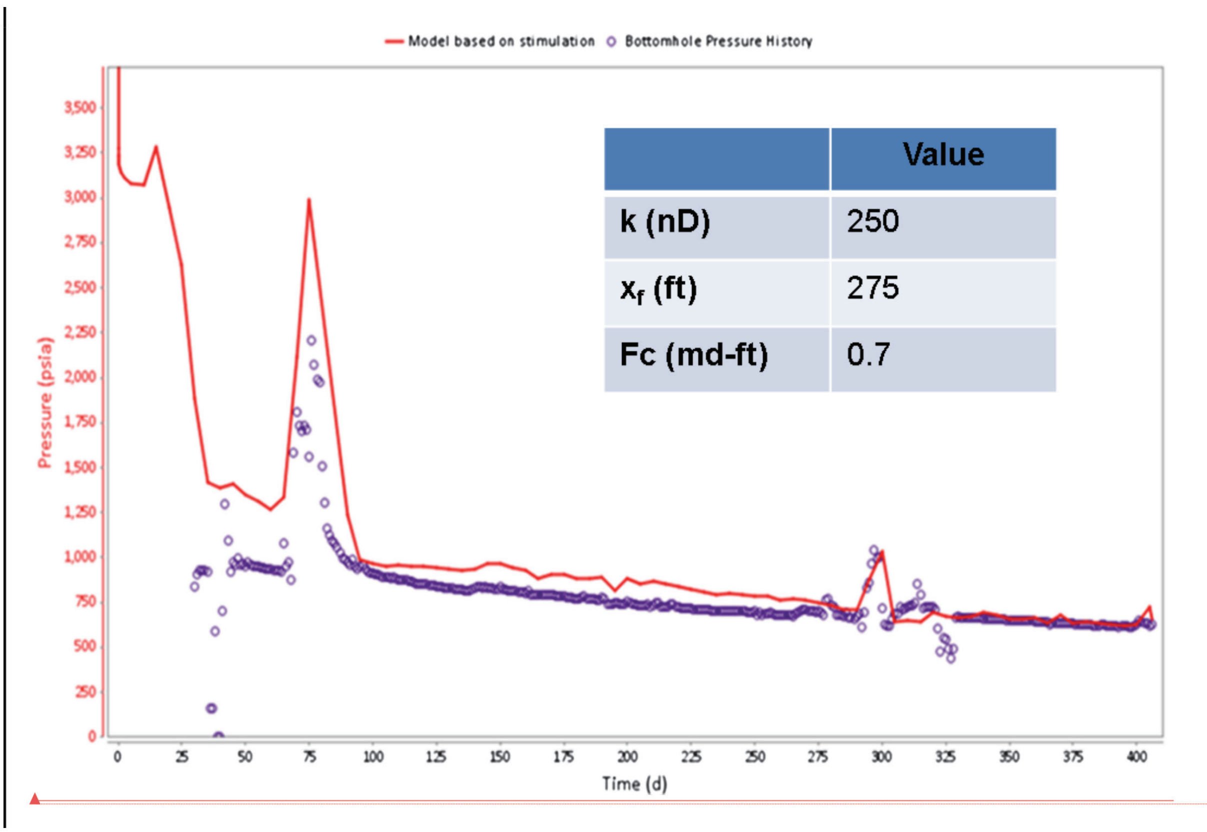

Figure 8. Performance match – Model based on geo-mechanical model.

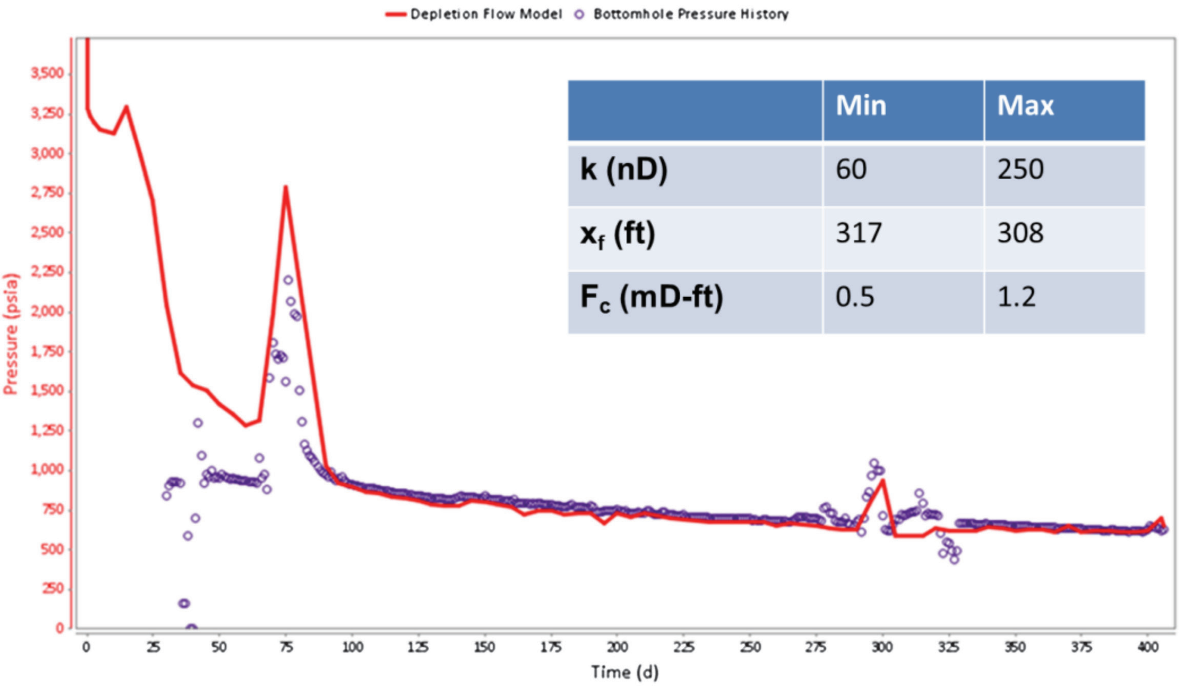

Figure 9. Adjusted history match with data performance.

Table 5 shows the stimulation output for the min and max frac area which contribute to flow using constant fracture geometry.

Stg	Half Length (ft)		Avg Fracture Height (ft)				Fracture Area (ft^2)	
	Min	Max	Hamilton	Marcellus	Onondaga	Total	Min	Max
1	308	317	189		11	340	628,320	646,680
2	308	317	189	140	11	340	628,320	646,680
3	308	317	189	140	11	340	628,320	646,680
4	308	317	189	140	11	340	628,320	646,680
5	308	317	189	140	11	340	628,320	646,680
6	308	317	189	140	11	340	628,320	646,680
7	308	317	189	140	11	340	628,320	646,680
8	308	317	189	140	11	340	628,320	646,680
9	308	317	189	140	11	340	628,320	646,680
10	308	317	189	140	11	340	628,320	646,680
11	308	317	189	140	11	340	628,320	646,680
12	308	317	189	140	11	340	628,320	646,680
Min Frac Area			7,539,840		Max Frac Area		7,760,160	

Table 5. Fracture geometry after performance analysis.

After the calibration performance, the final fracture geometry was adjusted to include constrains from fracture modeling and Microseismic observation. These final results are presented in Table 6. Yellow rows in Table 6, are the calibration results of the constrained fracture geometry (Table3) and fracture geometry after performance analysis (Table 5).

Stg	Half Length(ft)		Ave Fracture Height(ft)				Fracture Area(ft^2)	
	Min	Max	Hamilton	Marcellus	Onondaga	Total	Min	Max
1	0	0	0	0	0	0	0	0
2	308	317	189	140	11	340	628,320	646,680
3*	38	317	189	140	11	340	418,880	431,120
4	308	317	189	140	11	340	628,320	646,680
5	308	317	189	140	11	340	628,320	646,680
6	308	493	189	140	11	340	628,320	1,005,720
7	308	317	189	140	11	340	628,320	646,680
8	308	317	189	140	11	340	628,320	646,680
9	308	573	189	140	11	340	628320	1,168920
10	308	406	189	140	11	340	628,320	828,240
11	308	317	189	140	11	340	628,320	646,680
12*	308	317	189	140	11	340	418,880	431,120
Constrained Frac Area, ft^2					**7,745,200**			

* *Only 2 clusters contributing*

Table 6. Final fracture geometry after all constrains analysis.

Fracture Design Optimization

For this specific well, optimization stage was evaluated based on neighboring wells behavior. Figure 10 and Figure 11 presents the shale specific productivity index as a function of proppant mass and number of clusters for several wells. Results show that it could be beneficial to benefit use more proppant and more number of clusters per stage to increase productivity for the study well.

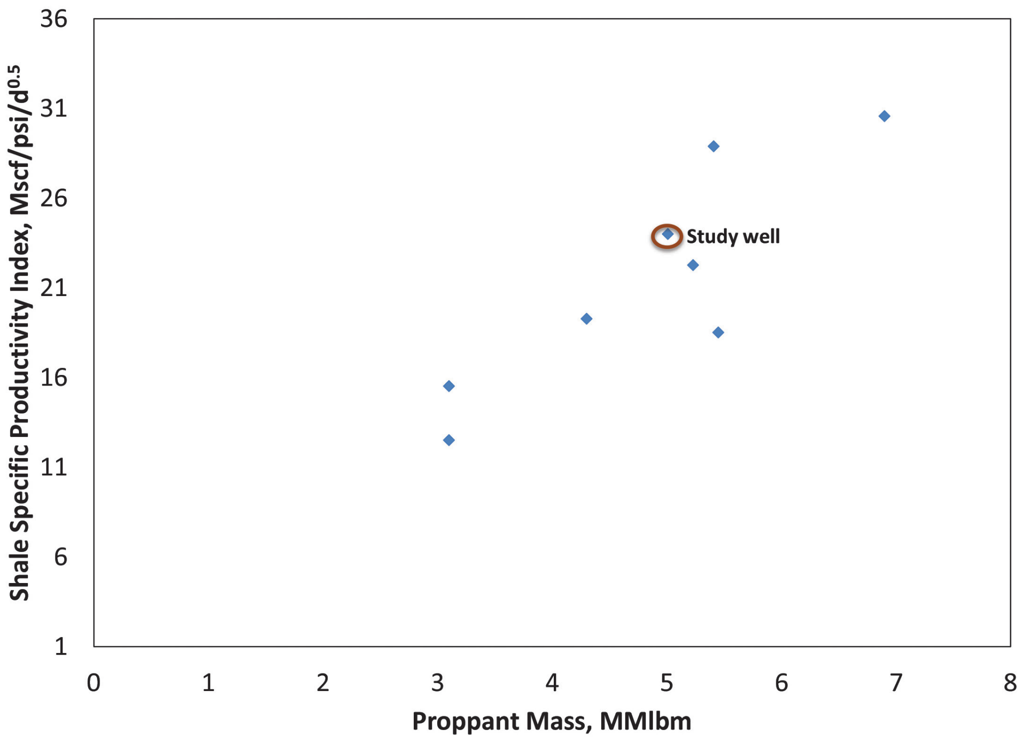

Figure 10. Shale specific productivity index as a function of proppant mass.

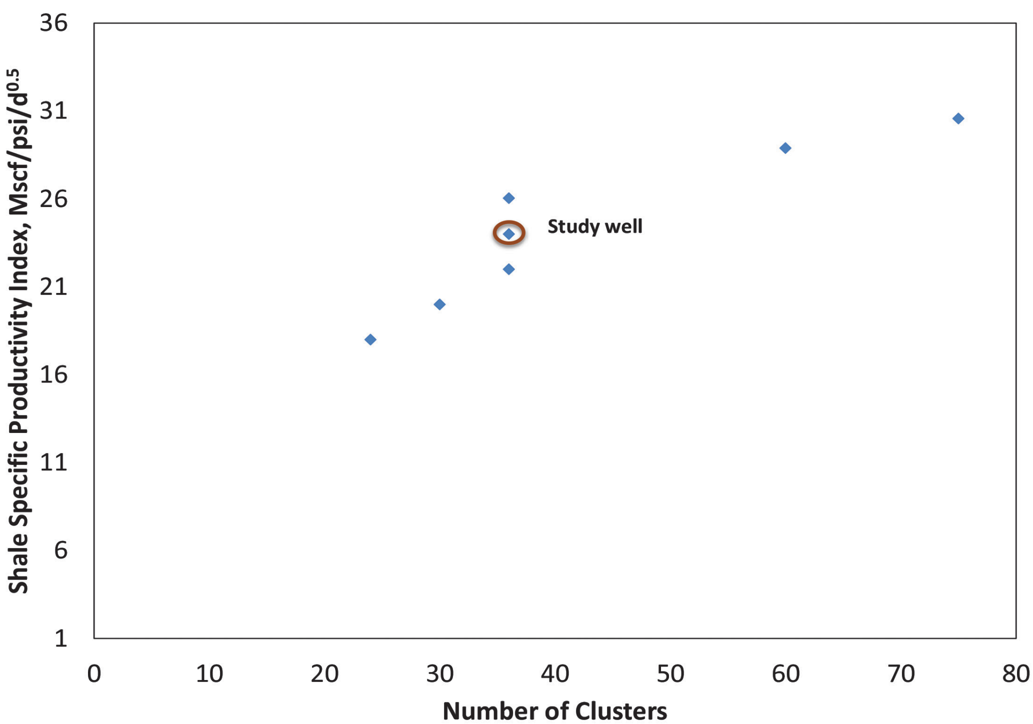

Figure 11. Shale specific productivity index as a function of number of clusters.

CONCLUSIONS

This work presents an integrated approach that spans from the formation evaluation to the post frac evaluation to optimize fracture designs. As we observed from this case, over- or underestimate fracture geometry could result in false prediction in reservoir properties, including reservoir permeability, EUR, and the estimated stimulated reservoir volume (SRV).

Proper understanding of the reservoir and rock quality is an essential step before performing fracture optimization work. If the fracture-to-fracture interference was not accurately predicted, false understandings of reservoir properties will result in overestimating/underestimating the ultimate recovery (EUR).

By integrating different data sources as constrains, a more accurate model is built that provides a better relationship between effective fracture geometry and reservoir permeability for the studied field.

REFERENCES

Roberts, C.N., 1981, Fracture Optimization In A Tight Gas Play: Muddy "J" Formation, Wattenberg Field, Colorado, paper SPE-9851-MS.

Ventura, J.L. and Slator Ranch, 1985, Fracture Optimization Study, paper SPE-12816-PA.

Richardson, Michael, 2000, A New and Practical Method for Fracture Design and Optimization, paper SPE-59736-MS.

Soliman, M.Y., Byrd, Audis, Walters, Harold, Weijers and Leen, 2004, Reservoir-Based Fracture Optimization Approach, paper SPE-86991-MS.

Agiddi, David Onimisi, 2005, A Decision Analysis Approach to Hydraulic Fracture Optimization in the W31S Stevens Oil Zone, Elk Hills Field, California, paper SPE-93989-MS.

Rahman, Md. Motiur, Rahman and Khalil, 2006, An Intelligent Hydraulic Fracture Optimization Model: A New Tool to Stimulate Low Permeable Oil Reservoir, paper SPE-101137-MS.

Jamiolahmady, Mahmoud; Sohrabi, Mehran; Mahdiyar, Hojjat, 2009, Optimization of Hydraulic Fracture Geometry, paper SPE-123466-MS.

Cipolla, Craig L.; Weng, Xiaowei; Onda, Hitoshi; Nadaraja, Thilaga; Ganguly, Utpal; Malpani, Raj, 2011, New Algorithms and Integrated Workflow for Tight Gas and Shale Completions, paper SPE-146872-MS.

Pitakbunkate, Termpan; Yang, Mei; Valko, Peter P.; Economides, Michael John, 2011, Hydraulic Fracture Optimization with a p-3D Model, paper SPE-142303-MS.

Rahman, M. Motiur; Sarma, Hemanta Kumar, 2011, Maximizing Tight Gas Recovery through a New Hydraulic Fracture Optimization Model, paper SPE-148205-MS.

Shebl, Mamdouh; Yalavarthi, Ramakrishna; Nyaaba, Clement, 2012, The Role of Detailed Petrophysical Reservoir Characterization in Hydraulic Fracture Modeling of Shale Gas Reservoirs, paper SPE-160341-MS.

Yang, Mei, 2012, Hydraulic Fracture Production Optimization With a Pseudo-3D Model in Multilayered Lithology, paper SPE-149833-MS.

Jin, C.J.; Sierra, Leopoldo; Mayerhofer, Mike, 2013, A Production Optimization Approach to Completion and Fracture Spacing Optimization for Unconventional Shale Oil Exploitation, paper SPE-168813-MS.

Brake, Albert C, 2013, Fracture Optimization in a Giant Gas Field, Wamsutter, Wyoming, USA, paper SPE-164029-MS.

Taylor, Robert; Hards, Eric; Fyten, Glen; Hoch, Ottmar F; Storozhenko, Ken; Stobo, Barry; Niebergall, Greg, 2013, Optimization of Duvernay Fracture Design Workflow, paper SPE-167238-MS.

Saldungaray, P.; Palisch, T., 2013, Hydraulic Fracture Optimization In Unconventional Reservoirs, paper OMC-2013-190.

Ugueto, Gustavo A.; Ehiwario, Michael; Grae, Abram; Molenaar, Mathieu; Mccoy, Kelly; Huckabee, Paul; Barree, Bob, 2014, Application of Integrated Advanced Diagnostics and Modeling To Improve Hydraulic Fracture Stimulation Analysis and Optimization, paper SPE-168603-MS.